metals

MDPI

Article

Microstructure and Corrosion Behavior of Extruded Mg-Sn-Y Alloys

Devadas Bhat Panemangalore [1], Rajashekhara Shabadi [2,3,4,5,*], Manoj Gupta [6] and Ludovic Lesven [7]

1 Department of Metallurgical and Materials Engineering, National Institute of Technology Karnataka, Surathkal 575025, India; devadasbhatp@nitk.edu.in
2 UMR 8207—UMET—Unité Matériaux et Transformations, Université de Lille, 59000 Lille, France
3 CNRS, UMR 8207 UMET, 59000 Lille, France
4 INRAE, 59000 Lille, France
5 Centrale Lille, 59000 Lille, France
6 Department of Mechanical Engineering, National University of Singapore, Singapore 117576, Singapore; mpegm@nus.edu.sg
7 UMR 8516—LASIR—Laboratoire de Spectrochimie Infrarouge et Raman, CNRS, Université de Lille, 59000 Lille, France; ludovic.lesven@univ-lille.fr
* Correspondence: rajashekhara.shabadi@univ-lille.fr; Tel.: +33-(0)-320-33-62-24

Abstract: Magnesium and its alloys, with their unique properties such as high strength/density ratio, good castability, and machinability, have found several applications in the aerospace and automotive industries. One of the reasons that restrict their widespread applicability is their poor corrosion resistance since Mg is readily oxidized in the presence of oxygen and humidity. The oxide layer is pseudo-passive and non-protective. The present effort tried to improve the passivity of this layer with the addition of alloying elements such as Tin (Sn) and Yttrium (Y) to create phases that interact differently with the oxidizing environment, thereby improving the corrosion resistance. In this work, the corrosion behavior of pure magnesium and Mg-5Sn-xY (x = 0.5, 1, 2 wt.%) were evaluated using immersion and potentiodynamic polarization tests. XRD, SEM-EDS, and EBSD have investigated the microstructure and elemental composition of the alloys. The present study is focused on elucidating the microstructure-corrosion relationship in Mg-Sn-Y alloys.

Keywords: magnesium; Mg-Sn-Y; corrosion

check for updates

Citation: Panemangalore, D.B.; Shabadi, R.; Gupta, M.; Lesven, L. Microstructure and Corrosion Behavior of Extruded Mg-Sn-Y Alloys. *Metals* **2021**, *11*, 1095. https://doi.org/10.3390/met11071095

Academic Editor: Soran Birosca

Received: 10 June 2021
Accepted: 6 July 2021
Published: 9 July 2021

Publisher's Note: MDPI stays neutral with regard to jurisdictional claims in published maps and institutional affiliations.

Copyright: © 2021 by the authors. Licensee MDPI, Basel, Switzerland. This article is an open access article distributed under the terms and conditions of the Creative Commons Attribution (CC BY) license (https://creativecommons.org/licenses/by/4.0/).

1. Introduction

Magnesium and its alloys have attracted enormous attention in the past few decades in the automotive and aerospace sectors over aluminum and its alloys because of their low density among engineering materials and have attractive specific strength [1]. But the high electrochemical activity of pure magnesium masks several beneficial properties it possesses. Several magnesium alloys like AZ (AZ31, AZ91, etc.) and AM (AM50, AM60, etc.) series, LAE443, AE42, are developed with nominal additions of aluminum to improve their corrosion resistance over pure magnesium. However, they suffer from poor high-temperature properties [2]. This is because of poor microstructural stability due to the softening of the $Mg_{17}Al_{12}$ phase. Therefore, one solution to this problem could be alloying with Tin (Sn), which is known to resist heat by forming Mg_2Sn [3] and has excellent creep characteristics [4] and good corrosion resistance [5,6]. The addition of low wt.% Sn could minimize the corrosion rate by several orders of magnitude [7]. This phase has high thermal stability, and it is expected to enhance high-temperature properties [8].

The addition of tin has been considered to have a beneficial influence in the biomedical implants based on magnesium [6,9,10] As-extruded Mg-1Sn and Mg-3Sn were synthesized by Zhao et al., and it did not induce toxicity to MG63 cells and was proved to be promising as biodegradable orthopedic implants [6]. Tang et al. studied the effect of Zn content on the microstructure and mechanical properties of indirect-extruded Mg-5Sn-xZn alloys.

They found that Mg_2Sn and MgZn type phases were responsible for better comprehensive mechanical properties [11]. Mg_2Sn-Mg composites were synthesized by Fang et al., and they exhibited excellent hardness, compressive strength, and ductility due to the nanophase reinforcement [12].

The low difference in the atomic radii between Yttrium (Y) and Mg makes Yttrium an excellent solid solution hardener [13]. Yttrium reduces the axis ratio of magnesium, leading to activation of other deformation modes like pyramidal slip in the case of extrusion at elevated temperature, resulting in enhanced ductility [14]. Yttrium has the standard electrode potential (SHE) almost the same as Mg, around –2.372 V [15]. Zhang et al. [16] elucidated the corrosion behavior of different as-cast Mg-Y alloys in NaCl solution. They found that with the addition of 15 wt.% Y, the amount of the second phase $Mg_{24}Y_5$ exceeded so much that it acts as a barrier for further corrosion. But with solutionizing heat treatment [17], the $Mg_{24}Y_5$ dissolved into the matrix, increasing the concentration of Y in the matrix and the corrosion rate. The mode of corrosion after solutionizing was filiform corrosion, and in as-cast, it propagates via pitting. For the electrochemical behavior of Mg-Y alloys, Sudholz et al. [18] studied several Mg-Y intermetallics and found that $Mg_{24}Y_5$ has an E_{corr} value which is 40–50 mV nobler than pure Mg.

Moreover, retardation of anodic reaction kinetics is possible with Y entering the solid solution. Pilling-Bedworth ratio (PBR) gives an insight into the protectiveness of the oxide layer. This ratio is less than one as the oxide coating layer is too thin and likely broken for pure magnesium. Rare-earth elements Y and Sn have PBR of 1.39 and 1.32, respectively, and it helps provide a passivating surface to protect against further surface oxidation. As compared to pure Mg and AZ31, Mg-Sn-Y and Mg-Y alloys exhibited better oxidation resistance due to Y-enriched oxide films on the surface [19].

This paper aims to investigate the corrosion behavior of as-extruded new Mg-5Sn-xY (x = 0.5, 1 and 2 wt.%) alloys and develop a microstructural relationship to explain the corrosion mechanism.

2. Materials and Methods

2.1. Materials

Mg turnings (ACROS Organics, Carlsbad, CA, USA) of 99.9+ % purity were used as the matrix material. The alloying addition Sn in powder form (325 mesh) and Mg-30Y master alloy (Company Name: Sunrelier Metal Co, Limited, Shanghai, China) were used to fabricate Mg-Sn-Y alloys.

2.2. Synthesis

Liquid-based synthesis technique by disintegrated melt deposition (DMD) method was used to produce pure Mg, Mg-5Sn, and Mg-5Sn-xY (x = 0.5, 1 and 2 wt.%) alloys [20]. This technique of synthesis results in a good yield and fine grain size. Ingots of diameter = 40 mm were machined to 36 mm. These ingots were extruded at 350 °C using a 150-ton hydraulic press into rods of 8 mm diameter after soaking at 400 °C for 1 h. These extruded rods were further used for several characterization methods. Elaborate characterization was carried out on samples that were cut in both transverse and longitudinal sections. Physical, electrochemical, and microstructural characterization was made on these extruded samples.

2.3. Microstructural Characterization

To study the texture and identify the presence of secondary phases, we used X-ray Diffraction (XRD) studies along transverse and longitudinal sections of extruded rods of the developed Mg alloys. The XRD characterization of the samples was done using a Rigaku SMARTLAB multipurpose diffractometer (Rigaku Corporation, Tokyo, Japan) (Operating Conditions: 9 kW rotating anode, operated at 45 kV and 200 mA) in Parallel Beam mode, delivering CuKα radiation (λ = 1.5418 Å). Then, $2\theta/\Omega$ scans were conducted between 20° and 100° with a scan speed of 3°/min and a 0.01° step size. Longitudinal

sections of the samples for microstructural characterization were first polished from 320 till 4000 grit SiC abrasive papers. For fine polishing, they were polished till 0.25 µm diamond paste. They were later polished using an SEM-Ion mill (Fischione, Export, PA, USA) to remove fine scratches and strain gradients on the surface. ZEISS optical microscope(ZEISS, Oberkochen, Germany) and JEOL Scanning Electron Microscope (SEM) (JEOL Ltd., Tokyo, Japan) coupled with Energy Dispersive Spectroscopy (EDS) (JEOL Ltd., Tokyo, Japan) were used for the microstructural studies. For quantitative microstructural analysis and to identify the orientation (texture) of the alloys, Electron Back Scattered Diffraction (EBSD) is used. The SEM was coupled with Oxford Instruments (Abingdon, UK) EDS/EBSD coupled system (80 mm^2 SDD Spectrometer and HKl Nordlys Max2 EBSD camera).

2.4. Microhardness

Microhardness measurements were performed on the as-polished transverse sections of Mg-Sn-Y samples using BUEHLER digital Microhardness tester. A Vickers indenter with a load of 500 gf and 15 s dwell time was used to conduct the microhardness tests following the ASTM: E384-11e1 [21]. The tests were performed for 15 repeatable readings.

2.5. Electrochemical Behavior

Electrochemical studies were conducted using the VOLTALAB (Radiometer analytical SAS, Lyon, France) instrument. The three-electrode setup was used as an electrochemical cell. Saturated calomel electrode as a reference electrode, platinum as a counter electrode, and the transverse section of the sample mounted inside a resin as the working electrode. Potentiodynamic polarization (PDP) tests were performed using VOLTALAB. The electrolyte used was 3.5% NaCl dissolved in 100 mL of de-ionized water at a temperature of 25 °C. The scan rate adopted was 1 mV/s ranging across the potential from −2.5 V to +2.5 V. For every test sample, a minimum of three trials were conducted. Before subjecting the samples to the test, they were polished using fine SiC abrasive papers and then washed with ethanol. SEM coupled with EDS was used to observe the microstructure and the composition of corroded products of corroded samples. Along with PDP tests, immersion tests for 48h were also carried out using the same solution.

3. Results

3.1. Microstructural Characterization

3.1.1. X-ray Diffraction

Figure 1 shows the XRD pattern of the extruded Mg and its alloys containing Sn and Y in transverse and longitudinal directions. With the incorporation of 5Sn into pure Mg, the X-ray analyses indicated Mg_2Sn in all the alloys. These peaks had low intensity, and it could be because of the low amount of Mg_2Sn. There were no ternary phases detected with small amounts of Y. XRD along the transverse section for the alloys showing maximum intensity for prismatic planes. The basal planes have very minimum intensity.

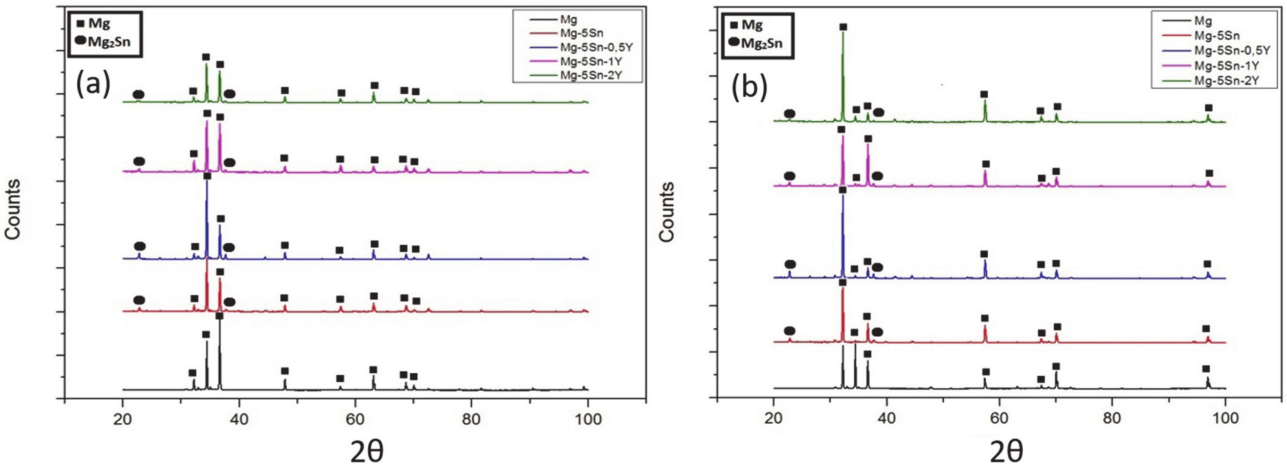


Figure 1. XRD diffractograms of as-extruded pure Mg and Mg-5Sn-xY (x = 0, 0.5, 1 and 2 wt.%) alloys along (**a**) longitudinal and (**b**) transverse direction.

The relative intensities are tabulated in Table 1.

Table 1. X-ray diffractogram intensities (T-Transverse and L-Longitudinal).

Material	Section	(I/I_{max}) Plane		
		$(10\bar{1}0)$ Prismatic	(0002) Basal	$(10\bar{1}1)$ Pyramidal
Mg	T	0.9602	1.0000	0.6295
	L	0.1546	0.6959	1.0000
Mg-5Sn	T	1.0000	0.0407	0.3407
	L	0.1329	1.0000	0.6379
Mg-5Sn-0.5Y	T	1.0000	0.0351	0.1285
	L	0.759	1.0000	0.4367
Mg-5Sn-1Y	T	1.0000	0.0581	0.8495
	L	0.2355	1.0000	0.9500
Mg-5Sn-2Y	T	1.0000	0.0649	0.1018
	L	0.1686	1.0000	0.9014

3.1.2. Optical Microscopy

The recorded optical micrographs of Mg and its alloys are given in Figure 2. Grain size values calculated from these microstructures using ImageJ software are tabulated in Table 2. Pure Mg consisted of equiaxed grains, and the alloys comprised secondary phases of different sizes and shapes aligned in the extrusion direction. These phases existed mostly along the grain boundaries, and the grain sizes of the alloys were finer than pure magnesium. The grain size decreased with the addition of Sn and Y, but the addition of Y alone did not greatly affect grain refinement. This was also the case for as-extruded Mg-1Sn-xY (x = 1.5, 3, 3.5 at.%) alloys synthesized by Zhao et al. [22]. Higher amounts of Y (x = 5.09, 9.68, and 11.1 wt.%) led to an increment of grain size from 6 to 12 μm [22]. But since the amount of Y is within 2 wt.%, the grain size values were less. These longitudinal sections had extrusion lines that could be seen in the microstructure.

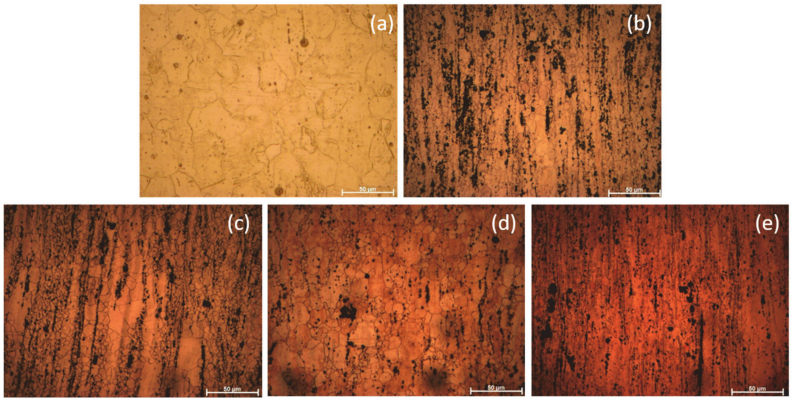


Figure 2. Optical microstructures of (**a**) Pure Mg (**b**) Mg-5Sn (**c**) Mg-5Sn-0.5Y (**d**) Mg-5Sn-1Y and (**e**) Mg-5Sn-2Y.

Table 2. Hardness and grain size values for pure Mg and Mg-5Sn-xY (x = 0, 0.5, 1 and 2 wt.%) alloys.

Material/Alloy	Hardness (hv 500)	Grain Size (μm)
Pure Mg	33.8	22.42
Mg-5Sn	51.75	3.62
Mg-5Sn-0.5Y	46.05	7.21
Mg-5Sn-1Y	47.65	5.92
Mg-5Sn-2Y	48.23	3.65

3.1.3. Scanning Electron Microscopy

Figure 3 depicts the backscattered electron (BSE) images of Mg-5Sn-xY (x = 0, 0.5, 1 and 2 wt.%) alloys. It consisted of secondary phases oriented mostly in the extrusion direction. These phases were present both inside and along the grain boundaries. Several morphologies were identified, and they were of rod-shaped and polygonal-shaped particles. Similar results were seen for Mg-Sn alloys with minor additions of Cu and Ag by previous researchers [23]. The polygonal-shaped particles were mostly Mg_2Sn type, and with the addition of Y, the number of such polygonal-shaped particles decreased. This was evident in the XRD, where the intensity for Mg_2Sn decreases with the addition of Y. In Mg-5Sn-2Y, the complex rod-shaped particles of type ($Mg_{83}Sn_1Y_{16}$) were hardly seen, and instead, several submicron globular shaped particles of type ($Mg_{75}Sn_2Y_{23}$) were seen distributed homogeneously.

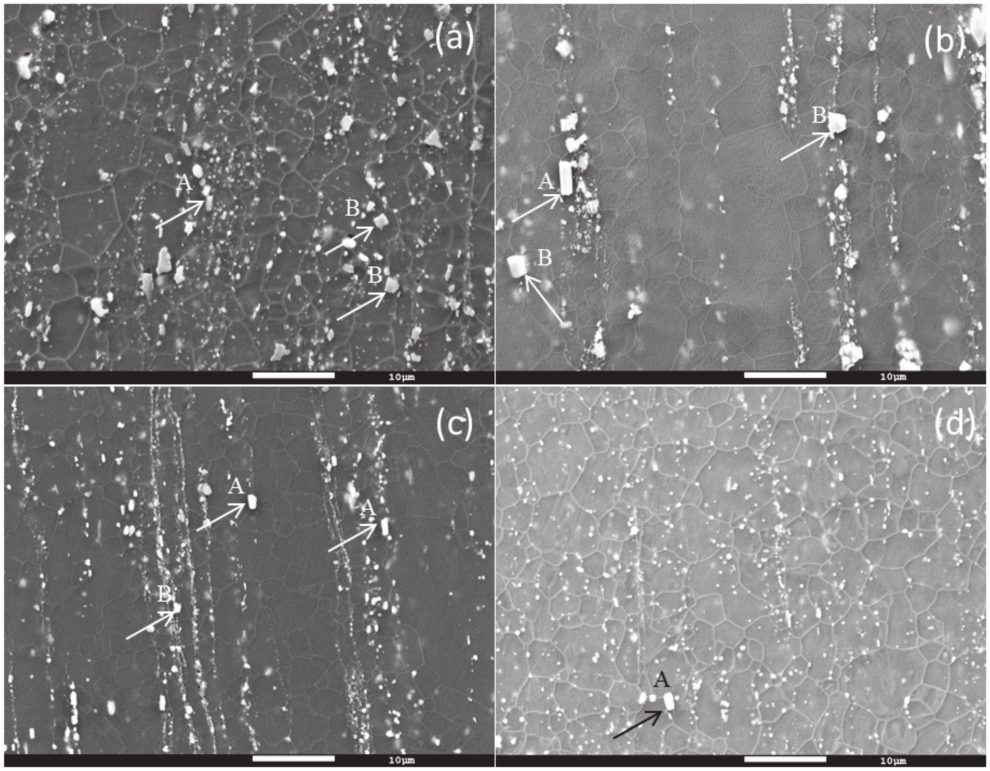


Figure 3. Scanning electron micrographs of (**a**) Mg-5Sn (**b**) Mg-5Sn-0.5Y (**c**) Mg-5Sn-1Y and (**d**) Mg-5Sn-2Y. (A = Oblong/Rod shaped and B = Polygonal).

3.1.4. Energy Dispersive Spectroscopy

Table 3 shows the compositional analysis of Mg-Sn-Y alloys using energy dispersive spectroscopy. It could be seen from the table that the rod-shaped particles were rich in magnesium. With the addition of Y, the Mg content in these particles decreased. Whereas for the polygonal type particles, the composition of these secondary phases belonged to the same range, and they resembled the type $Mg_2(Sn,Y)$.

Table 3. EDS spot analysis of the secondary phases present in Mg-Sn-Y alloys (all values are in wt.%).

Material	Oblong/ Rod (A)	Polygonal (B)
Mg-5Sn	(93)Mg-(7)Sn	(76)Mg-(24)Sn
Mg-5Sn-0.5Y	(88)Mg-(6)Sn-(5)Y	(49)Mg-(26)Sn-(24)Y
Mg-5Sn-1Y	(71)Mg-(15)Sn-(13)Y	(55)Mg-(23)Sn-(21)Y
Mg-5Sn-2Y	(56)Mg-(2)Sn-(41)Y	(41)Mg-(29)Sn-(29)Y

3.1.5. Electron Back-Scattered Diffraction

Figure 4 depicts the inverse pole figure (IPF) of as-extruded pure Mg and Mg-5Sn-2Y extruded at 350 °C with the observation direction parallel to the longitudinal (extruded) direction using SEM-EBSD. Pure Mg showed a basal texture. The addition of Sn and Y to Mg further strengthened the basal texture, as seen in Figure 4. The maximum intensity of basal poles for Mg-5Sn-2Y (35 m.u.d) was higher than for pure Mg (10 m.u.d). There is a difference in the distribution of poles between pure Mg and Mg-5Sn-2Y. The basal poles with the maximum intensities were oriented slightly towards (~20°) the TD from ND for pure Mg. For Mg-5Sn-2Y, they were oriented towards (~60°) the ED from the ND. The strengthening of basal texture could be due to the presence of second-phase particles due to the addition of alloying elements. Texture strengthening due to the addition of Sn to Mg was also seen by She et al. [24]. Additionally, a considerable decrease in the grain size could be seen with the addition of alloying elements.

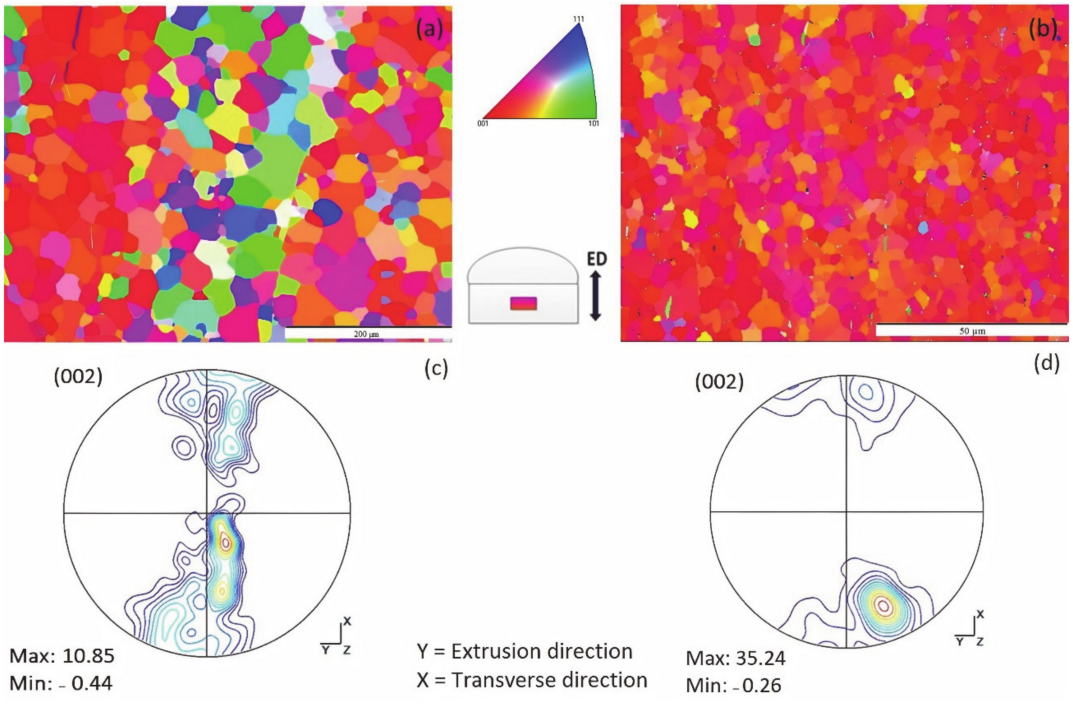


Figure 4. IPFs of (**a**) Pure Mg (**b**) Mg-5Sn-2Y along with their corresponding PFs in (**c**) and (**d**), respectively.

3.2. Microhardness

The Vickers hardness measurements of pure magnesium and its alloys are shown in Table 2. It can be observed that for Mg-5Sn alloy, there is a notable increase in the microhardness value as compared to pure magnesium. The Mg-5Sn alloy exhibited a maximum hardness (51.75 hv 500) value. This could be due to the high hardness value of the secondary phase Mg_2Sn [25]. The ternary phases do not contribute to an added hardness value for Mg-Sn-Y alloys. This could be due to the minimal additions of Y that resulted in a small number of ternary phases.

3.3. Corrosion Behavior

3.3.1. Weight Loss

Figure 5 depicts the weight-loss measurements of Mg, Mg-5Sn, and Mg-5Sn-xY (x = 0.5, 1 and 2 wt.%) samples. After 48 h of immersion in 3.5 wt.% NaCl, a significant amount of corrosion products was formed on all the specimens, especially pure magnesium. A lot of corrosion products were skimmed out of the material and into the solution. These powder sediments made the color of the solution cloudy. It could be seen that the weight loss rate of these samples increased in this order of Mg-5Sn-xY < Mg-5Sn < Pure Mg. Hence the corrosion resistance decreases in the same order. Pure Mg suffered a 44% weight loss after 2 days of immersion. But the weight loss for Mg-5Sn-0.5Y was the least among all the materials, and it was only 3%. With substantial corrosion occurring in all the specimens, it was concluded that the time of 48h was too severe.

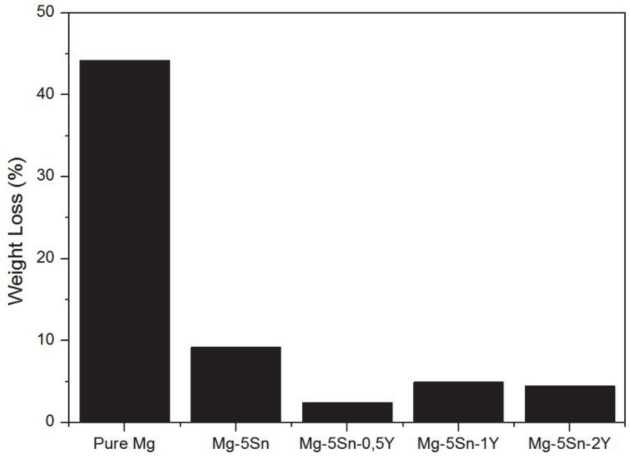


Figure 5. Immersion test results for pure Mg and Mg-5Sn-xY (x = 0, 0.5, 1 and 2 wt.%) alloys.

The corrosion morphologies for pure Mg and Mg-5Sn-0.5Y after immersing for 48 h in 3.5 wt.% NaCl solution and cleaning with chromic acid are seen in Figure 6. Large pits could be seen for pure Mg, which were deep, and the corrosion process was initiated from the edges. Corrosion occurred throughout the sample. Whereas for Mg-5Sn-0.5Y, filiform-type corrosion occurred. Also, there were small pits observed. Since the second phases were not seen, they may have got dissolved during immersion. This could also be seen for corrosion of Mg-7Sn alloys, where the type of Sn distribution in the microstructure decides the corrosion mechanism [26]. If more Sn in the solution form in the matrix, then filiform corrosion mode activates, and if Sn is present as Mg_2Sn throughout, then pitting corrosion takes over, which is more detrimental, as observed by Liu et al. [26]. With 5 wt.% Sn addition and not many pits could be seen after 48h immersion, it could be concluded that the corrosion process was not severe for the alloys with Sn and Y additions.

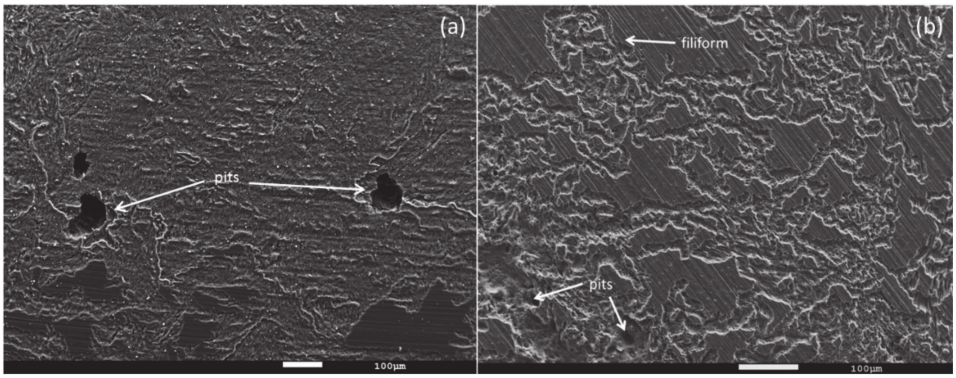


Figure 6. Corrosion morphology of (**a**) Pure Mg and (**b**) Mg-5Sn-0.5Y.

3.3.2. Potentiodynamic Polarization Test

Figure 7 depicts the potentiodynamic polarization curves for the developed Mg-Sn-Y alloys in 3.5 wt.% NaCl solution. Pure Mg is plotted for reference. Here, the current response is plotted as a function of the applied potential, and the polarization characteristics are measured. The potential was applied from the cathodic region that corresponds to the H_2 evolution reaction to the anodic region where Mg dissolution occurs. While moving the corrosion potential towards E_{corr}, the corrosion current density decreased for all the samples. For Mg-5Sn, the value of cathodic current density is high. This means that at the onset of immersion, there existed an accelerated cathodic hydrogen evolution. In the graph, a shift in the positive direction for corrosion potential could be seen for increasing amounts of Y. Both anodic and cathodic branches shift to lower current densities with an increase in Y content. Table 4 demonstrates the corrosion properties of E_{corr} (vs Ag/AgCl)

and i_{corr} values derived from this polarization plot. These values were calculated using the Tafel extrapolation method, i.e., by intersecting the slopes of anodic and cathodic curves.

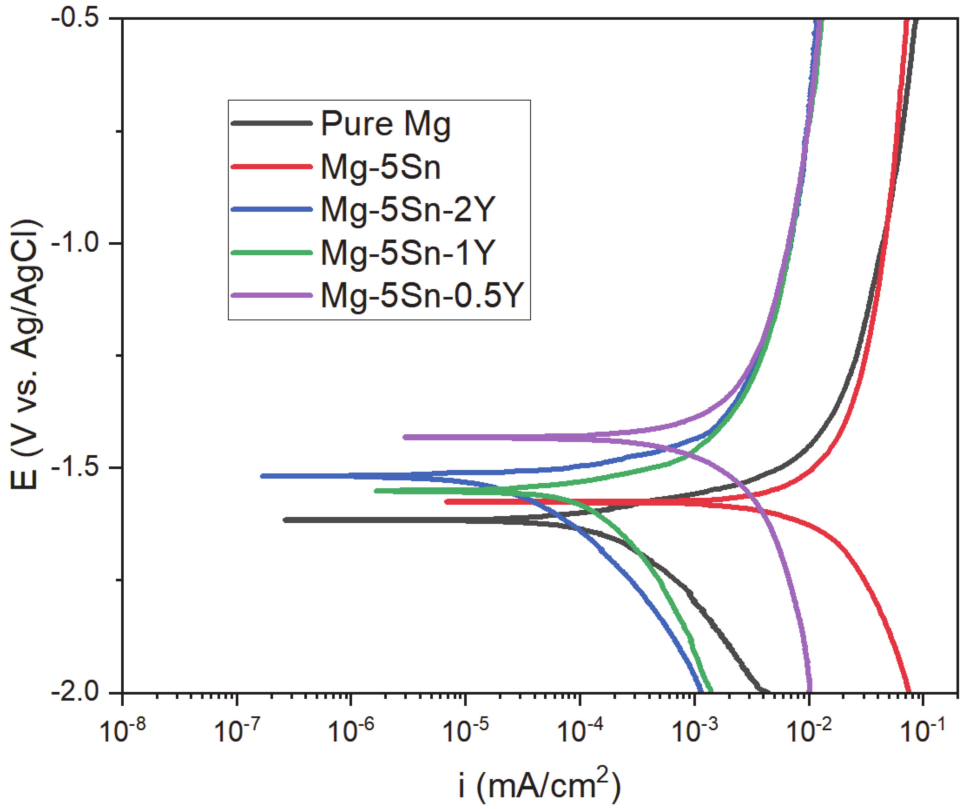


Figure 7. Potentiodynamic Polarization test results for Mg-5Sn-xY (x = 0, 0.5, 1 and 2 wt.%) alloys.

Table 4. Measurements related to corrosion rate in 3.5 wt.% NaCl solution at room temperature.

Material	E_{corr} (V vs. Ag/AgCl)	i_{corr} ($mAcm^{-2}$)
Mg-5Sn	−1.57	0.2
Mg-5Sn-0.5Y	−1.425	0.04
Mg-5Sn-1Y	−1.55	0.15
Mg-5Sn-2Y	−1.51	0.25

4. Discussions

The solid solubility of Sn in Mg is 14.48 wt.%, and for Y, it is 11.4 wt.% [27]. Mg-xSn alloys were synthesized by Zhao et al. who studied the strain hardening behavior of as-extruded alloys, and they also found fiber texture [28]. They have attributed the PSN effect to the decreased grain size and an inhomogeneous microstructure. MgO formed on the surface has a mismatch with the pure Mg surface underneath. The addition of alloying elements reduced the grain size that could increase the corrosion resistance of magnesium alloys [29]. Due to a large number of grain boundaries, the porosity generated through the supply of vacancies gets transported easily and eases the surface film stress [30].

Moreover, the addition of these elements leads to an increased number of second phases, which has a collective influence on the corrosion rate of the alloys. These phases are precipitated during hot-extrusion that led to the generation of several dislocations and subgrain boundaries. A similar observation has been reported by Chen et al. in extruded Mg-Sn alloys [31]. This can enhance the passivity of the film to some extent.

The corrosion behavior of Mg-Sn-Y alloys was studied in great detail. With the PDP tests, it is evident that the addition of Y has enhanced the corrosion resistance. Also, the weight loss measurements and PDP tests are in good agreement. All the measurements

were taken because there were no detectable impurities on the extruded samples that could influence the results. When Mg-Sn-xY alloys were immersed in NaCl solution, the material degradation occurred as per the following reaction:

$$Mg + 2H_2O \rightarrow Mg(OH)_2 + H_2 \uparrow \quad (1)$$

This reaction can be split into two partial anodic and cathodic reactions and they are represented as follows:

$$Mg \rightarrow Mg^{2+} + 2e^- \quad (2)$$

$$2H_2O + 2e^- \rightarrow H_2 + 2OH^- \quad (3)$$

With time, $Mg(OH)_2$ develops on the partially protective surface. This film gets dissolved by the presence of strong chloride anions.

Zhao et al. [6] found an increase in corrosion rate with increasing Sn addition to Mg. Although the grain size became finer, it also resulted in a greater number of secondary phase Mg_2Sn and led to form galvanic couples with α-Mg. This is because the secondary phases have more positive potential, and hence, it acts as a cathode, and the α-matrix acts as an anode—tests on Hanks solution for 1, 3, 5, and 7 wt.% Sn additions to Mg were carried out, and Mg-1Sn exhibited the lowest corrosion rate [6]. Heon-Young Ha et al. studied the effect of tin in the electrochemical behavior of extruded Mg-5 wt.% Sn alloy. They found the inhibition of the cathodic reaction in the Mg-5Sn alloy compared to Mg [32]. The secondary phases in Mg-Sn-Y alloys here are uniformly distributed, and their volume fraction is not high. Hence their effect is less detrimental for corrosion attacks.

The corrosion rate of alloys with the addition of Y has reduced. This could be because element Y can be distributed in the oxide film. The increasing addition of Y increased the corrosion potential to a positive value. This could also be seen in Mg-Y alloys with increasing Y content from 1–5 wt.% as studied by Liu et al. [33]. Moreover, the addition of rare-earth elements like Y can exhibit special properties of negating the influence of impurity elements like Fe by forming intermetallics. This phenomenon is also known as the 'scavenger effect.' Pilling-Bedworth ratio of Y_2O_3 is greater than 1; the oxide film formed on the surface during corrosion can act as a passivating surface. Tremendous research is underway in synthesizing the corrosion-resistant Mg-based alloys and composites [34].

5. Conclusions

Mg-Sn and Mg-Sn-Y impurity-free alloys were prepared using the disintegrated-melt-deposition (DMD) technique, which was followed by hot-extrusion. The microstructural analysis showed that the alloys were composed of α-Mg, Mg_2Sn, and ternary phases of the type $Mg_xSn_rY_z$. The alloys underwent dynamic recrystallization during the extrusion process and exhibited finer grain sizes. The addition of Sn and Y enhanced the hardness, and it is attributed to the finer grain size and the presence of the harder secondary phase Mg_2Sn. EBSD analysis showed that extruded pure Mg exhibited a typical basal texture, whereas Mg-5Sn-2Y exhibited a stronger basal texture. Mg-Sn-Y alloys also exhibited lower corrosion rates, and Mg-5Sn-0.5Y exhibited the lowest weight loss and corrosion current density in immersion test results and potentiodynamic polarization tests, respectively. Due to the presence of Sn and Y that led to more passivity of the film, it reduced the corrosion speed of Mg-Sn-Y alloys. Moreover, the presence of Y in the oxide film can reduce corrosion.

Author Contributions: Conceptualization, D.B.P. and R.S.; Methodology, D.B.P., R.S. and M.G.; Data Curation, D.B.P. and L.L.; Writing—Original Draft Preparation, D.B.P.; Writing—Review & Editing, D.B.P. and R.S.; Supervision, R.S. All authors have read and agreed to the published version of the manuscript.

Funding: This research received no external funding.

Institutional Review Board Statement: Not applicable.

Informed Consent Statement: Not applicable.

Data Availability Statement: Not applicable.

Acknowledgments: D.B.P. sincerely thanks University Lille doctoral research grant for supporting his graduate program. The SEM national facility in Lille (France) is supported by the Conseil Regional du Hauts-de-France and the European Regional Development Fund (ERDF).

Conflicts of Interest: The authors declare no conflict of interest.

References

1. Luo, A.A. Magnesium casting technology for structural applications. *J. Magnes. Alloy.* **2013**, *1*, 2–22. [CrossRef]
2. Avedesian, M.M.; Baker, H. *ASM International Handbook Committee: Magnesium and Magnesium Alloys*; ASM International: Novelty, OH, USA, 1999; ISBN 9780871706577.
3. Son, H.T.; Lee, J.B.; Jeong, H.G.; Konno, T.J. Effects of Al and Zn additions on mechanical properties and precipitation behaviors of Mg-Sn alloy system. *Mater. Lett.* **2011**, *65*, 1966–1969. [CrossRef]
4. Bowles, A.L.; Dieringa, H.; Blawert, C.; Hort, N.; Kainer, K.U. Investigations in the Magnesium-Tin System. *Mater. Sci. Forum* **2005**, *488–489*, 135–138. [CrossRef]
5. Hou, L.; Li, Z.; Zhao, H.; Pan, Y.; Pavlinich, S.; Liu, X.; Li, X.; Zheng, Y.; Li, L. Microstructure, Mechanical Properties, Corrosion Behavior and Biocompatibility of As-Extruded Biodegradable Mg–3Sn–1Zn–0.5Mn Alloy. *J. Mater. Sci. Technol.* **2016**, *32*, 874–882. [CrossRef]
6. Zhao, C.; Pan, F.; Zhao, S.; Pan, H.; Song, K.; Tang, A. Preparation and characterization of as-extruded Mg–Sn alloys for orthopedic applications. *Mater. Des.* **2015**, *70*, 60–67. [CrossRef]
7. Kubásek, J.; Vojtěch, D.; Lipov, J.; Ruml, T. Structure, mechanical properties, corrosion behavior and cytotoxicity of biodegradable Mg-X (X = Sn, Ga, In) alloys. *Mater. Sci. Eng. C* **2013**, *33*, 2421–2432. [CrossRef]
8. Jayalakshmi, S.; Arvind Singh, R.; Thenambika, V.; Kirubanidhi, J.; Gupta, M. Impression Creep Characteristics of Mg-Sn-Ag Alloy. *Appl. Mech. Mater.* **2016**, *854*, 33–37. [CrossRef]
9. Zhao, W.; Wang, J.; Weiyang, J.; Qiao, B.; Wang, Y.; Li, Y.; Jiang, D. A novel biodegradable Mg-1Zn-0.5Sn alloy: Mechanical properties, corrosion behavior, biocompatibility, and antibacterial activity. *J. Magnes. Alloy.* **2020**, *8*, 374–386. [CrossRef]
10. Zhen, Z.; Xi, T.; Zheng, Y.; Li, L.; Li, L. InVitro study on Mg-Sn-Mn Alloy as biodegradable metals. *J. Mater. Sci. Technol.* **2014**, *30*, 675–685. [CrossRef]
11. Tang, W.N.; Park, S.S.; You, B.S. Effect of the Zn content on the microstructure and mechanical properties of indirect-extruded Mg–5Sn–xZn alloys. *Mater. Des.* **2011**, *32*, 3537–3543. [CrossRef]
12. Fang, C.; Wen, Z.; Liu, X.; Hao, H.; Chen, G.; Zhang, X. Microstructures and mechanical properties of Mg2Sn-nanophase reinforced Mg–Mg2Sn composite. *Mater. Sci. Eng. A* **2017**, *684*, 229–232. [CrossRef]
13. Zhang, J.H.; Liu, H.F.; Sun, W.; Lu, H.Y.; Tang, D.X.; Meng, J. Influence of structure and lonic radius on solubility limit in the Mg-Re systems. *Mater. Sci. Forum* **2007**, *561–565*, 143–146. [CrossRef]
14. Sugamata, M.; Hanawa, S.; Kaneko, J. Structures and mechanical properties of rapidly solidified Mg-Y based alloys. *Mater. Sci. Eng. A* **1997**, *226–228*, 861–866. [CrossRef]
15. Gerischer, H. Elektrodenpotentiale: Tables of Standard Electrode Potentials. Hrsg. von G. Milazzo und S. Caroli. John Wiley & Sons: Chichester, New York, 1978. XVI, 421 S., geb. £ 17,50. *Nachr. Chem. Tech. Lab.* **1978**, *26*, 661. [CrossRef]
16. Zhang, X.; Zhang, K.; Deng, X.; Hongwei, L.; Yongjun, L.; Minglong, M.; Ning, L.; Wang, Y. Corrosion behavior of Mg–Y alloy in NaCl aqueous solution. *Prog. Nat. Sci. Mater. Int.* **2012**, *22*, 169–174. [CrossRef]
17. Zhang, X.; Zhang, K.; Li, X.; Deng, X.; Li, Y.; Ma, M.; Shi, Y. Effect of solid-solution treatment on corrosion and electrochemical behaviors of Mg-15Y alloy in 3.5 wt.% NaCl solution. *J. Rare Earths* **2012**, *30*, 1158–1167. [CrossRef]
18. Sudholz, A.D.; Gusieva, K.; Chen, X.B.; Muddle, B.C.; Gibson, M.A.; Birbilis, N. Electrochemical behaviour and corrosion of Mg–Y alloys. *Corros. Sci.* **2011**, *53*, 2277–2282. [CrossRef]
19. Yu, X.; Jiang, B.; Yang, H.; Yang, Q.; Xia, X.; Pan, F. High temperature oxidation behavior of Mg-Y-Sn, Mg-Y, Mg-Sn alloys and its effect on corrosion property. *Appl. Surf. Sci.* **2015**, *353*, 1013–1022. [CrossRef]
20. Gupta, M.; Lai, M.O.; Saravanaranganathan, D. Synthesis, microstructure and properties characterization of disintegrated melt deposited Mg/SiC composites. *J. Mater. Sci.* **2000**, *35*, 2155–2165. [CrossRef]
21. ASTM. Standard Test Method for Knoop and Vickers Hardness of Materials. E384-11e1. Available online: http://www.astm.org/cgi-bin/resolver.cgi?E384-11e1 (accessed on 4 September 2018).
22. Zhao, H.D.; Qin, G.W.; Ren, Y.P.; Pei, W.L.; Chen, D.; Guo, Y. Microstructure and tensile properties of as-extruded Mg-Sn-Y alloys. *Trans. Nonferr. Met. Soc. China* **2010**, *20*, s493–s497. [CrossRef]
23. Jayalakshmi, S.; Sankaranarayanan, S.; Koh, S.P.X.; Gupta, M. Effect of Ag and Cu trace additions on the microstructural evolution and mechanical properties of Mg-5Sn alloy. *J. Alloys Compd.* **2013**, *565*, 56–65. [CrossRef]
24. She, J.; Pan, F.; Zhang, J.; Tang, A.; Luo, S.; Yu, Z.; Song, K.; Rashad, M. Microstructure and mechanical properties of Mg-Al-Sn extruded alloys. *J. Alloys Compd.* **2016**, *657*, 893–905. [CrossRef]
25. Kevorkijan, V.; Davor Skapin, S. Studies of Mg2Sn-based composites. *Assoc. Met. Eng. Serb.* **2010**, *16*, 47–61.

26. Liu, X.; Shan, D.; Song, Y.; Chen, R.; Han, E. Influences of the quantity of Mg2Sn phase on the corrosion behavior of Mg–7Sn magnesium alloy. *Electrochim. Acta* **2011**, *56*, 2582–2590. [CrossRef]
27. ASM International. *ASM Handbook, Volume 3, Alloy Phase Diagrams*; ASM International: Novelty, OH, USA, 2004; Volume 7, ISBN 0871703777.
28. Zhao, C.; Chen, X.; Pan, F.; Gao, S.; Zhao, D.; Liu, X. Effect of Sn content on strain hardening behavior of as-extruded Mg-Sn alloys. *Mater. Sci. Eng. A* **2018**, *713*, 244–252. [CrossRef]
29. Ralston, K.D.; Birbilis, N. Effect of Grain Size on Corrosion: A Review. *Corrosion* **2010**, *66*, 075005. [CrossRef]
30. Liao, J.; Hotta, M.; Yamamoto, N. Corrosion behavior of fine-grained AZ31B magnesium alloy. *Corros. Sci.* **2012**, *61*, 208–214. [CrossRef]
31. Chen, D.; Ren, Y.P.; Guo, Y.; Pei, W.L.; Zhao, H.D.; Qln, G.W. Microstructures and tensile properties of as-extruded Mg-Sn binary alloys. *Trans. Nonferr. Met. Soc. China* **2010**, *20*, 1321–1325. [CrossRef]
32. Ha, H.Y.; Kang, J.Y.; Yang, J.; Yim, C.D.; You, B.S. Role of Sn in corrosion and passive behavior of extruded Mg-5 wt%Sn alloy. *Corros. Sci.* **2016**, *102*, 355–362. [CrossRef]
33. Liu, X.; Shan, D.; Song, Y.; Han, E. Influence of yttrium element on the corrosion behaviors of Mg—Y binary magnesium alloy. *J. Magnes. Alloy.* **2017**, *5*, 26–34. [CrossRef]
34. Yang, Y.; Lu, C.; Shen, L.; Zhao, Z.; Peng, S.; Shuai, C. In-situ deposition of apatite layer to protect Mg-based composite fabricated via laser additive manufacturing. *J. Magnes. Alloy.* **2021**. [CrossRef]